



ARTICLE

WZ66, a novel acetyl-CoA carboxylase inhibitor, alleviates nonalcoholic steatohepatitis (NASH) in mice

Ying-sheng Gao¹, Min-yi Qian^{1,2}, Qiang-qiang Wei³, Xu-bin Duan¹, Shi-lei Wang⁴, Hai-yang Hu⁵, Jun Liu¹, Chu-yue Pan¹, Shuo-quan Zhang¹, Lian-wen Qi⁶, Jin-pei Zhou⁷, Hui-bin Zhang² and Li-rui Wang¹

The global prevalence of nonalcoholic steatohepatitis (NASH) increases incredibly. NASH ends up to advanced liver disease, which is highly threatening to human health. Currently, treatment of NASH is very limited. Acetyl-CoA carboxylases (ACC1/ACC2) are proved as effective drug targets for NASH. We aimed to develop novel ACC inhibitors and evaluate their therapeutic value for NASH prevention. ACC inhibitors were obtained through structure-based drug design, synthesized, screened from ACC enzymatic measurement platform and elucidated in cell culture-based assays and animal models. The lipidome and microbiome analysis were integrated to assess the effects of WZ66 on lipids profiles in liver and plasma as well as gut microbiota in the intestine. WZ66 was identified as a novel ACC1/2 inhibitor. It entered systemic circulation rapidly and could accumulate in liver. WZ66 alleviated NASH-related liver features including steatosis, Kupffer cells and hepatic stellate cells activation in diet-induced obese mice. The triglycerides (TGs) and other lipids including diglycerides (DGs), phosphatidylcholine (PC) and sphingomyelin (SM) were decreased in WZ66-treated mice as evidenced by lipidome analysis in livers. The lipids profiles in plasma were also altered with WZ66 treatment. Plasma TG were moderately increased, while the activation of SREBP1c was not detected. WZ66 also downregulated the abundance of *Allobaculum*, *Mucispirillum* and *Prevotella* genera as well as *Mucispirillum schaedleri* species in gut microbiota. WZ66 is an ideal lead compound and a potential drug candidate deserving further investigation in the therapeutics of NASH.

Keywords: nonalcoholic steatohepatitis; Acetyl-CoA carboxylase; WZ66; pharmacokinetics lipidome; gut microbiome

Acta Pharmacologica Sinica (2020) 41:336–347; <https://doi.org/10.1038/s41401-019-0310-0>

INTRODUCTION

Parallel to obesity, the prevalence of nonalcoholic steatohepatitis (NASH) has dramatically increased, and it is becoming the most common liver disease worldwide [1]. NASH had usually been developed on the basis of simple hepatic steatosis. However, in contrast to simple steatosis, NASH is characterized by obvious hepatocyte injury and death. Dying hepatocytes release cytokines or other factors to promote the infiltration of immune cells into the liver, inciting further injury and inflammation [2]. Meanwhile, dying hepatocytes produce morphogens that enrich the injured liver with regenerative cell types such as myofibroblasts, immune cells, and liver cell progenitors to trigger the wound healing process. Repetitive injury to the liver causes progressive scarring, leading to fibrosis and cirrhosis as well as a higher risk of liver cancer [3, 4]. The currently available therapies for NASH are limited to weight loss, vitamin E supplementation and pioglitazone. The global burden of NASH urgently awaits the development of effective therapies for this life-threatening disease.

Acetyl-CoA carboxylase (ACC) catalyzes the ATP-dependent carboxylation of acetyl-CoA to produce malonyl-CoA. This

reaction, which proceeds in two half-reactions, a biotin carboxylase (BC) reaction and a carboxyltransferase (CT) reaction, is accomplished by the cooperation of the BC, CT, and biotin carboxyl carrier protein (BCCP) domains of ACC [5, 6]. In mammals, ACC exists as two tissue-specific isozymes, ACC1, which is present in lipogenic tissues (liver, adipose), and ACC2, which is present in oxidative tissues (liver, heart, and skeletal muscle). The ACCs (ACC1 and ACC2), which are encoded by separate genes, display distinct cellular distributions and functions [7]. ACC1, together with ATP citrate lyase and fatty acid synthase, are key enzymes in the de novo lipogenesis (DNL) pathway. ACC2, a mitochondrial membrane-associated enzyme, generates malonyl-CoA primarily to inhibit carnitine palmitoyl-transferase and regulate fatty acid transport into the mitochondria [8, 9]. Thus, the combination of ACC1 and ACC2 inhibition may lead to decreased de novo fatty acid production and enhanced fatty acid oxidation (FAO), and therefore offer an attractive target for favorably affecting a multitude of health risk factors associated with NASH, diabetes, obesity, and cancer [5, 10–14].

¹School of Basic Medicine and Clinical Pharmacy, State Key Laboratory of Natural Medicines, China Pharmaceutical University, Nanjing 211198, China; ²College of pharmacy and chemistry, Dali University, Dali 671003, China; ³Center of Drug Discovery, State Key Laboratory of Natural Medicines, China Pharmaceutical University, Nanjing 210009, China; ⁴School of Traditional Chinese Pharmacy, State Key Laboratory of Natural Medicines, China Pharmaceutical University, Nanjing 211198, China; ⁵School of Life Science and Technology, China Pharmaceutical University, Nanjing 211198, China; ⁶Clinical Metabolomics Center, China Pharmaceutical University, Nanjing 211198, China and ⁷Department of Medicinal Chemistry, China Pharmaceutical University, Nanjing 211198, China

Correspondence: Hui-bin Zhang (zhanghb80@cpu.edu.cn) or Li-rui Wang (wanglirui@cpu.edu.cn)

These authors contributed equally: Ying-sheng Gao, Min-yi Qian, Qiang-qiang Wei

Received: 18 June 2019 Accepted: 12 September 2019

Published online: 23 October 2019

Here, we aimed to discover novel inhibitors of the ACCs and evaluate their activities and effects *in vitro* and *in vivo*. Lipidome analysis was utilized to examine the effects of the inhibitors on lipid profiles in the liver and plasma. Microbiome analysis was also employed to detect alterations in gut microbiota composition resulting from the inhibition of the ACCs because changes in gut microbiota are closely linked with the progression of NASH [15, 16]. This study extensively evaluated the consequences of ACC inhibitors on a variety of aspects related to NASH and was expected to provide a new lead compound or potential drug for NASH treatment.

MATERIALS AND METHODS

Animals

All animal care and experiments were performed according to the Laboratory Animal Management Regulations of China, guidelines of the China Pharmaceutical University Institutional Animal Care and Use Committee. Five-week-old C57BL/6J male mice (purchased from Beijing Vital River Laboratory Animal Technology Co., Ltd., China) were maintained on a 12 h light and 12 h dark cycle in a temperature/humidity-controlled and specific pathogen-free environment. To establish the model, mice had free access to a high-fat diet (Research Diet, D12492, USA) and water during all the procedures. This model can stimulate the metabolic characteristics of human NASH [17]. After 10 weeks of following high-fat diet feeding, mice were grouped randomly and intragastrically gavaged (ig) with vehicle, WZ66 (25 or 50 mg/kg) or PF-05175157 (50 mg/kg) every day, where PF-05175157 is an analog of WZ66 [18], from the 10th week to the end of experiment as described in Fig. 3a. PF-05175157 was purchased from MedChem-Express (HY-12942, USA). Food intake and body weights were recorded every week. After 22 weeks of HFD feeding, the mice were sacrificed, and the tissues including the blood, liver and cecum were harvested.

Design and synthesis of WZ66

The synthetic route with high to moderate yields for WZ66 is described in Scheme 1. Briefly, the commercially available 2,4-dihydroxyacetophenone (S4762, Selleck, USA) was reacted with isoprene in dioxane at room temperature (RT) to obtain intermediate 1. Intermediate 2 was prepared from intermediate 1 using *N*-(tert-butoxycarbonyl)-4-piperidone in the presence of pyrrolidine in methanol. Then, the key intermediate 3 was yielded by removing the Boc group of intermediate 2 by treatment with hydrochloric acid in ethyl acetate. Finally, WZ66 was synthesized via the classical method of amide formation involving the condensation between intermediate 3 and 4-methyl-2-*n*-propyl-1H-benzimidazole-6-carboxylic acid in dimethylformamide (DMF). Reagents and conditions: (a) isoprene, BF₃, dioxane, RT, 36 h; (b) pyrrolidine, methyl alcohol (MeOH), 80 °C, 10 h; (c) i. HCl gas, ethyl acetate, RT, 1 h; ii. 2 N NaOH aq, H₂O; (d) 4-methyl-2-*n*-propyl-1H-benzimidazole-6-carboxylic acid, HOBt, EDCI, Et₃N, DMF, 40 °C, 2 h.

Docking analysis

The crystal complex of the humanized yeast ACC CT domain (PDB ID: 5CTB) was obtained from the RCSB Protein Data Bank. The docking analysis was processed with the Glide docking protocol [19]. Hydrogen atoms were added to the structure, and the water was removed. Then, a 60 Å box centered on the geometrical center of the ligand binding site was generated for grid calculation. All ligand molecules were drawn in ChemDraw 2014 and saved as an sdf. Then, WZ66 was processed at a simulated pH of 7.4 ± 1.0 to generate all possible tautomers, stereoisomers, and protonation states and was finally minimized with the OPLS 2005 force field with the Ligand preparation protocol of Maestro 10.2 [20]. Once the docking analysis was complete, only one docking conformation was saved.

Enzymatic assay

ACC activity was measured using a luminescent ADP detection assay (ADP-Glo Kinase Assay Kit, Promega, USA) by quantifying ADP production during the first enzymatic half-reaction (Pharmaron, Beijing, China). Specifically, 4.5 µL of assay buffer containing either recombinant human ACC1 or ACC2 was added to each well of a 384-well OptiPlate (PerkinElmer) followed by the addition of 0.5 µL of DMSO or DMSO containing different concentrations of WZ66. The final concentration of WZ66 in the well increased in 3-fold increments from 0.85 to 50 000 µM. Another 5.0 µL of substrate mixture was subsequently added to each well to initiate the reaction. After 30 min of incubation at RT, 10 µL of ADP-Glo Reagent was added to terminate the reaction, and plates were incubated for 40 min to deplete the remaining ATP. Finally, 20 µL of Kinase Detection Reagent was added to each well, and the plate was incubated for another 40 min to convert the ADP to ATP, which was detected via a luciferin/luciferase reaction using a PerkinElmer EnVision 2104 plate reader.

Cell lines and primary hepatocyte cultures

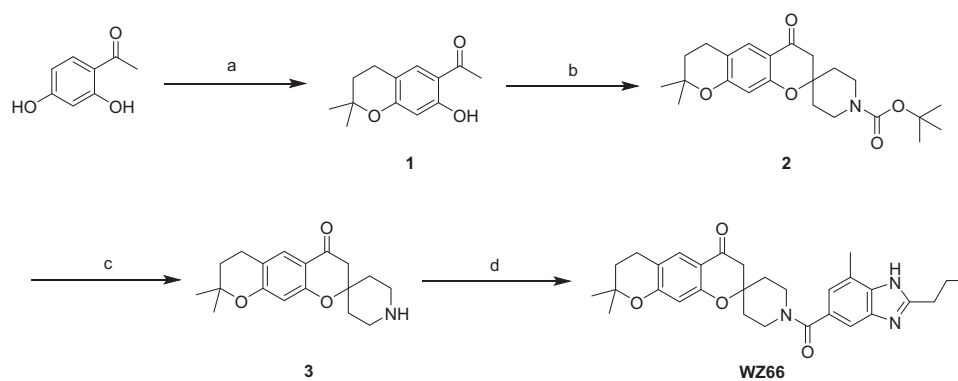
The mouse hepatocyte cell line AML12 (ATCC, CRL-2254) was cultured in DMEM/F12 medium (Gibco, 11330-032, USA) with 5 µg/mL insulin, 5 µg/mL transferrin, 5 ng/mL selenium, 40 ng/mL dexamethasone, 10% fetal bovine serum (FBS) (HyClone, SH30396.03, USA) and 1% anti-anti (Gibco, 15240-062). Primary hepatocytes were isolated from 8-week-old C57BL/6J male mice as reported in our previous work [21, 22]. Briefly, after anesthetization, mice were perfused through the inferior vena cava with SC-1 buffer (137 mM NaCl, 5.4 mM KCl, 0.7 mol/L NaH₂PO₄, 0.85 mM Na₂HPO₄, 10 mM HEPES, 2 mM NaHCO₃, 0.5 mM EGTA, and 5 mM glucose) via a 20G catheter needle. Once the perfusion started, the portal vein was cut off. When the liver turned light brown (approximately 3 min later), the perfusate was changed to SC-2 buffer (137 mM NaCl, 5.4 mM KCl, 0.7 mM NaH₂PO₄, 0.85 mM Na₂HPO₄, 10 mM HEPES, 2 mM NaHCO₃, and 3.8 mM CaCl₂) containing 0.5 g/L collagenase D and 50 mg/L collagenase P (Roche, USA) for 8 min. After perfusion, the liver was excised into a dish with 30 mL of ice-cold SC-2 buffer and suspended gently with forceps. The suspension was filtered through a 70 µm cell filter and centrifuged at 50 × *g* for 1 min at 4 °C. The cell pellet was washed with ice-cold SC-2 buffer and centrifuged again under the same conditions. The precipitate was resuspended in Medium 199 containing 10% FBS and 1% antibiotics. Cell viability was measured by 0.04% trypan blue solution. Cells were then cultured on collagen-coated plates, and the medium was changed to serum-free Medium 199 containing DMSO or WZ66 (1 µM) after approximately 2 h and incubated for another 24 h.

Palmitic acid induction of lipid droplets

AML12 cells were cultured in 12-well plates overnight, and the cells were then treated with 250 µM palmitic acid sodium salt for 24 h. Then, the cells were treated with vehicle (DMSO), 1 µM WZ66 or transfected with *Acaca* siRNA for another 24 h in serum-free medium. Each group had three wells of cells. After that, the cells were fixed with 4% paraformaldehyde for 15 min and rinsed in Oil red O solution for 30 min. After washing with water, the staining of the lipid droplets was observed under a microscope.

Cell transfection

AML12 cells were seeded in 12-well plates and cultured for 24 h before transfection. Mouse *Acaca* siRNAs (sense: 5'-GCAGGUUGC-CAACAUCUATT-3'; antisense: 5'-UAGGAUGUUGGCAUCUGCTT-3') and negative control siRNAs (sense: 5'-UUCUCCGAACGUGU CACGUTT-3'; antisense: 5'-ACGUGACACGUUCGGAGAATT-3') were purchased from GenePharma (Shanghai, China). One microgram of siRNA was used for the transfection.



Scheme 1 Synthesis route of WZ66

Real-time polymerase chain reaction

Total RNA was extracted with TRIZOL (TAKARA, 9109, Japan) and reverse transcribed with the High Capacity cDNA Reverse Transcription kit (ABI, 4368814, USA). Real-time quantitative polymerase chain reaction was performed as reported in a previously published paper [22], using SYBR Premix (Vazyme, Q331-02, China) according to the manufacturer's instructions in an ABI StepOnePlus instrument. The data were analyzed via the $\Delta\Delta Ct$ method and normalized to 18S mRNA. All primer sequences were designed by Primer3Plus (<http://www.primer3plus.com/>) and are listed in the Supplementary information.

Western blotting

Western blot analysis was performed as described in our previous work [22], using anti- β -actin (Sigma, A5441, USA) with 1:5000 dilution, anti- α -SMA (Abcam, ab5694, USA) and anti-SREBP1c (Abcam, ab28481) with 1:1000 dilution in 5% nonfat milk at 4 °C overnight followed by the corresponding secondary antibodies for 1 h at RT. Densitometry of the Western blot analysis was performed using ImageJ and normalized to β -actin under a double-blind control.

Liver and plasma lipidome

The lipidome in the liver and plasma from the vehicle and WZ66-treated mice were analyzed by liquid chromatography-mass spectrometry (LC-MS) as described in previous methods [23–25]. Briefly, a cold dichloromethane/methyl alcohol (DCM/MeOH, 3:1, v/v) solution containing an internal standard was added to the liver tissues, and the volume of the solution was determined based on the weight of the tissue (50 μ L of solution/mg tissue). Then, the liver tissues were homogenized with a beads-beater (Biospec Products, Inc., Bartlesville, OK, USA) followed by the addition of 300 μ L of distilled water. The solution was vortexed gently for 10 min and centrifuged (13 000 $\times g$, 10 min, 4 °C). The DCM layer was collected, dried and finally reconstituted in water/isopropanol/acetonitrile 5:30:65 (v/v/v) [23, 24]. For the plasma samples, 300 μ L of MeOH containing an internal standard was thoroughly mixed with 50 μ L of plasma. Methyl tert-butyl ether (MTBE) was used to extract the lipids in the plasma, and another 300 μ L of distilled water was subsequently added. The mixture was vortexed and centrifuged (10 min, 13 000 $\times g$, 4 °C), and the supernatant was finally evaporated and reconstituted in the buffer of the mobile phase as described below [24, 25].

The reconstituted samples from the liver and plasma were finally analyzed by a 1290 Infinity Ultra High-Performance Liquid Chromatography (HPLC) System and 6545 quadrupole time-of-flight mass spectrometer, which was equipped with a Dual Agilent Jet Stream electrospray source. MassHunter Data Acquisition software (version B.06.01) was used to run the whole system. Lipids were separated on a reversed-phase UPLC ACQUITY C8 BEH

column (Milford, MA, USA) (55 °C) in electrospray positive and negative ionization modes. The mobile phase was described as follows: water containing 10 mM ammonium acetate (negative mode) or 0.1% formic acid (positive mode) was used as mobile phase A, and 20% isopropanol in acetonitrile was used as phase B. The flow rate of the mobile phase was 0.3 mL/min followed by gradient elution.

The LC-MS raw data files generated from the system were transferred to mzData format using a DA preprocessor with a threshold of 2000 counts. The open-source software XCMS was adopted to perform peak finding, filtering and alignment. Lipid identification was accomplished based on MS/MS fragments, and the accurate mass was acquired via Lipid Maps (www.lipidmaps.org) [26].

Bacteria genome analysis (16S ribosomal RNA)

The cecum contents were collected, and the total bacterial genomic DNA was extracted as described in our previous study [22]. The 16S rRNA gene (V1–V3 region) was amplified and sequenced by the Illumina MiSeq platform [22, 27] in Annoroad Gene Technology Co (Beijing, China) and analyzed by QIIME2 [28]. The raw data have been deposited in the NCBI Sequence Read Archive (SRA) database (accession no. PRJNA527923).

Pharmacokinetics and tissue biodistribution assay

Pharmacokinetics: C57BL/6J male mice ($n = 4$), which were 5 weeks old, were set up for the assay. Peripheral blood was collected and transferred to anticoagulant tubes 0.25, 0.5, 1, 2, 4, 8, 12, and 24 h after the dosing of WZ66 (ig, 50 mg/kg). Samples were immediately centrifuged and stored at -20 °C until detection. Next, 300 μ L of methanol was added to 50 μ L of plasma. The mixture was vortexed and centrifuged at 12 000 $\times g$ for 10 min at 4 °C. The supernatant was evaporated and reconstituted in 100 μ L methanol. The concentration of WZ66 in plasma was determined by HPLC. HPLC analysis was performed with a reversed-phase column (SYMMETRY SHIELD RP 18, 4.6 mm \times 250 mm i.d., 5 μ m, Waters Co., USA). The mobile phase consisted of acetonitrile and 0.05% formic acid in water (v/v). The analyte was detected with a fluorescence detector (set at a wavelength of 214 nm). The calibration curves of WZ66 ranged from 0.1 to 50 μ g/mL with correlation coefficients > 0.999. The pharmacokinetic parameters of WZ66 from individual mice were calculated with Phoenix WinNonlin 6.1 (Pharsight Corporation, Mountain View, CA, USA).

Tissue biodistribution assay: C57BL/6J male mice ($n = 8$), which were 5 weeks old, were set up for the assay. Mice were given WZ66 by gavage at a dose of 50 mg/kg. At 4, 8, 12, and 24 h after administration, the mice were sacrificed, and the tissues (liver, kidney, lung, spleen, muscle, heart, fat, and brain) were collected at each time point ($n = 2$). After being ground, the WZ66 in the tissues was extracted with 500 μ L of acetonitrile and analyzed using HPLC as described above.

Histology

Livers were fixed in formalin, embedded in paraffin, sectioned and stained for hematoxylin-eosin staining [22]. Frozen livers were sectioned and used for Oil red O staining [22]. Liver sections for sirius red staining were performed as described [21]. Sections were scanned with a Nanozoomer 2.0 RS.

Immunofluorescence

Immunofluorescent staining for F4/80 was carried out as described in our previous study [22]. Briefly, frozen liver sections were rinsed in phosphate-buffered saline (PBS) for 5 min 3 times. Then, the sections were incubated with DAKO protein block (S3022, DAKO, Denmark) for 30 min at RT. Sections were covered with anti-F4/80 at a 1:200 dilution (eBioscience, 14-4801-82, USA) at 4 °C overnight. Sections were washed 3 times with PBS for 5 min and incubated with goat anti-rat secondary antibody (Invitrogen, A11077, USA) at a 1:200 dilution for 60 min at RT. Sections were rinsed 3 times with PBS for 2 min each time and mounted with DAKO fluorescent mounting media (S3023, DAKO).

Immunohistochemistry

Paraffin-embedded liver sections were deparaffinized by xylene and concentration gradients of ethyl alcohol. Antigens were retrieved using an antigen unmasking solution (Vector Laboratories, H-3300, USA). The sections were permeabilized with 0.3% Triton X-100 for 30 min and immersed in 1% H₂O₂ for 30 min. After blocking with 5% goat serum in 0.5% bovine serum albumin for 30 min, the liver sections were incubated with an α -SMA primary antibody (Abcam, ab5694) overnight at 4 °C. Sections were then washed with PBS and incubated with a biotin-labeled secondary antibody and ABC solution (Vector Laboratories, PK-6101) for 30 min, respectively. Finally, the sections were stained with DAB solution (Vector Laboratories, SK-4105) for 25 min.

Kit assays

Total cholesterol (A111-1), HDL-c (A112-1), and LDL-c (A113-1) in plasma were measured using kits from Nanjing Jiancheng Bioengineering Institute. Malonyl-CoA in AML12 cells after treatment with 1 μ M WZ66 for 24 h was detected with a kit from MyBioSource (MBS705127, USA). All kit assays were performed according to the manufacturers' instructions.

Data and statistical analysis

For 16S rRNA gene sequencing, the significance of the differential abundance of the genus and phylum levels between the groups was estimated via a negative binomial test of the edgeR R package after TMM normalization, and the Benjamini & Hochberg corrected $P < 0.05$ was considered significantly different. Significances in the lipidome heatmap were estimated by Student's t test. A one-way ANOVA with the Newman-Keuls multiple comparison test was used to analyze the significant differences between multiple groups. All other results were analyzed using the Mann-Whitney test with GraphPad Prism 5.0. Values are presented as the mean \pm SEM, and differences with P values < 0.05 were considered statistically significant.

RESULTS

WZ66 was identified as a novel ACC1/2 inhibitor

The structure of WZ66 (Fig. 1a) was designed based on the compound that was in complex with the humanized yeast ACC CT domain in PDB: 5CTB. The direct interaction between WZ66 and ACC was examined by docking analysis (Fig. 1b) and confirmed in the enzymatic activity assay (Fig. 1c). Indeed, WZ66 inhibited the enzymatic activities of both ACC1 and ACC2 with IC₅₀ values of 435.9 and 141.3 nM (Fig. 1c), respectively. Consistently, we found that treatment of WZ66 in AML12 mouse hepatocytes resulted in a 25% decline in malonyl-CoA levels relative to control cells (Fig. 1d).

As expected, WZ66 decreased palmitic acid-induced lipid accumulation in AML12 cells, as revealed by Oil red O staining (Fig. 1e). We also demonstrated extensive reduced gene expression of DNL-related genes, especially fatty acid biosynthesis and sphingolipid biosynthesis, while increased gene expression of lipolysis-related genes in WZ66-treated AML12 cells and mouse primary hepatocytes was revealed by the reduction in acetyl-coA carboxylase alpha (*Acaca*), *Acacb*, fatty acid synthase (*Fasn*), glycerol-3-phosphate acyltransferase (*Gpam*), ceramide synthase (*Cers4*) and *Cers6* gene expression as well as an increase in patatin-like phospholipase domain containing 3 (*Pnpla3*) gene expression (Fig. 1f). Furthermore, we knocked down the gene expression of *Acaca* in AML12 cells to confirm that inhibitory effects of WZ66 on lipogenesis was mediated by ACC1 (Supplemental Fig. 1a). We found that knockdown of *Acaca* decreased lipid accumulation, which is consistent with a previous report [11]; nevertheless, WZ66 failed to significantly inhibit lipogenesis in cells with si*Acaca* compared with vehicle treatment, suggesting that prevention of lipogenesis by WZ66 was mediated at least in part by ACC1 (Fig. 1g). Collectively, the above results indicated that WZ66 blocked lipid accumulation by functioning as a novel ACC1/2 inhibitor.

Pharmacokinetics and tissue biodistribution of WZ66 in mice

Before evaluating the in vivo efficacy of WZ66, we detected the pharmacokinetic and tissue biodistribution of this compound in vivo. For this purpose, mice were given WZ66 by gavage at a dose of 50 mg/kg, and the plasma concentration of WZ66 reached a peak value after 2 h with a C_{max} of 7.35 μ g/mL (Fig. 2a). In addition, the tissue biodistribution results demonstrated that WZ66 preferentially accumulated in the liver compared with other tissues, including the kidney, lung, spleen, muscle, heart, fat, and brain (Fig. 2b). Notably, the detected value of WZ66 in the brain approached an undetectable level, indicating that it did not cross the blood-brain barrier easily (Fig. 2b). Overall, our results suggested that WZ66 was absorbed into systemic circulation quickly and could accumulate in the liver where the target ACC1/2 is abundantly located.

WZ66 alleviated hepatic steatosis, prevented the activation and infiltration of macrophages and decreased hepatic stellate cell activation

Mice were fed a HFD and treated with WZ66 and PF-05175157 as depicted in Fig. 3a. Food intake and the body weights of WZ66-treated mice did not differ significantly from those in the vehicle group (Fig. 3b). However, the liver weights and liver/body weight ratios of WZ66-treated mice were significantly reduced compared with the vehicle group (Fig. 3c). We next demonstrated that WZ66 decreased lipid accumulation and hepatic steatosis in a dose-dependent manner, as revealed by H&E and Oil red O staining (Fig. 3d). Notably, the extent of reduction in hepatic steatosis induced by WZ66 (50 mg/kg) was higher than that of PF-05175157 (50 mg/kg) (Fig. 3d).

Furthermore, WZ66 treatment decreased the expression of liver F4/80 and several chemokines, such as *Cxcl2* and *Cxcl10* (Fig. 4a, b), indicating that WZ66 could possibly prevent both macrophage activation and infiltration, while PF-05175157 failed to prevent the activation of macrophages. We also revealed that WZ66 inhibited *Col1a1* gene expression and collagen accumulation in the liver (Fig. 4c), which was not observed in PF-05175157-treated mice. α -SMA gene expression and protein levels were also lower in the WZ66-treated group relative to the vehicle group, suggesting that hepatic stellate cell activation was prevented by WZ66 (Fig. 4c, e). The expression of all genes was normalized to the vehicle group to control unwanted sources of variation. Taken together, WZ66 effectively decreased liver weight, hepatic steatosis, liver fibrosis, and macrophage activation and infiltration in HFD-induced obese mice.

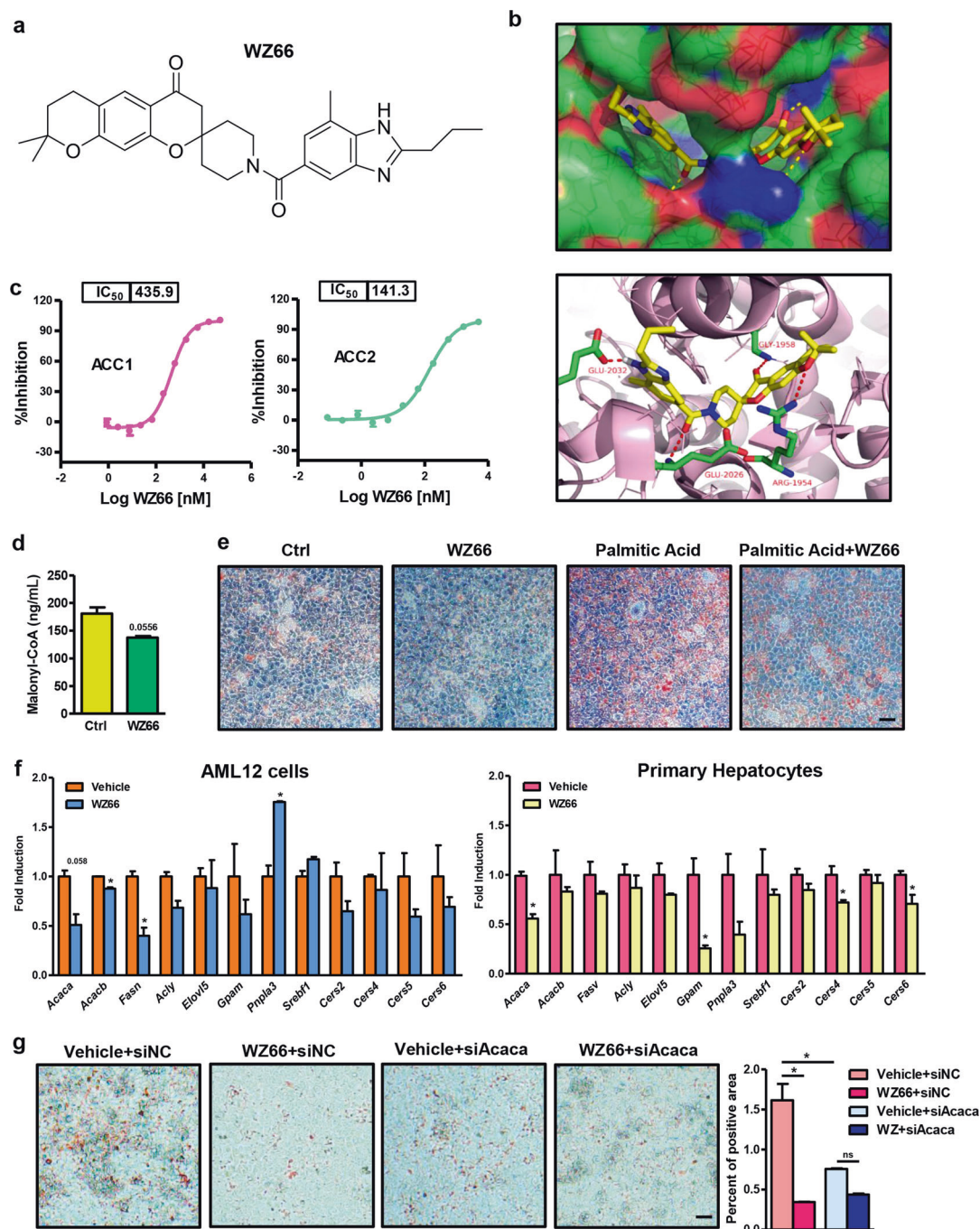


Fig. 1 Identification of WZ66 as a novel ACC1/2 inhibitor. **a** Chemical structure of WZ66. **b** Model of WZ66 bound to the CT domain of humanized yeast ACC. Images depict a docked model of WZ66 and CT domain of ACC (PDB ID: 5CTB). **c** Inhibition of the ACC1 and ACC2 enzymatic activities by WZ66. Assays were performed in three independent experiments. **d** Malonyl-CoA concentration in AML12 cells treated with vehicle (Ctrl) or WZ66 (1 μ M) for 24 h. **e** Representative images of Oil red O staining of AML12 cells. Cells were induced with palmitic acid (250 μ M) for 24 h and treated with vehicle or WZ66 for another 24 h (scale bar = 50 μ m, magnification = 100 \times). **f** (left) *Acaca*, *Acacb*, *Fasn*, *Acly*, *Elovl5*, *Gpam*, *Pnpla3*, *Srebf1*, *Cers2*, *Cers4*, *Cers5*, *Cers6* mRNA expression in AML12 cells treated with vehicle or WZ66; (right) *Acaca*, *Acacb*, *Fasn*, *Acly*, *Elovl5*, *Gpam*, *Pnpla3*, *Srebf1*, *Cers2*, *Cers4*, *Cers5*, *Cers6* mRNA expression in primary hepatocytes treated with vehicle or WZ66. * $P < 0.05$. **g** (left) Representative images of Oil red O staining of AML12 cells. After induction with palmitic acid (250 μ M) for 24 h, AML12 cells were transfected with siRNA (siNC: negative control siRNA; siAcaca: *Acaca* siRNA) and treated with WZ66 (1 μ M) for another 24 h (scale bar = 50 μ m, magnification = 40 \times); (right) quantification of Oil red O staining. * $P < 0.05$. Experiments were repeated in three independent experiments. Data are represented as the mean \pm SEM

Lipidome analysis in the livers of WZ66-treated mice
Untargeted lipidome analysis was performed to investigate the alterations in lipid composition in the livers of WZ66-treated mice. As presented in Fig. 5a, a total of 244 lipid species were identified

in the livers, involving 16 classes, including carotenoids (Cars), ceramides (Cers), coenzyme Q9, diglycerides (DGs), free fatty acids (FFAs), lysophosphatidylcholine (LysoPC), lysophosphatidylethanolamine (LysoPE), monoglycerides (MGs), phosphatidic acid (PA),

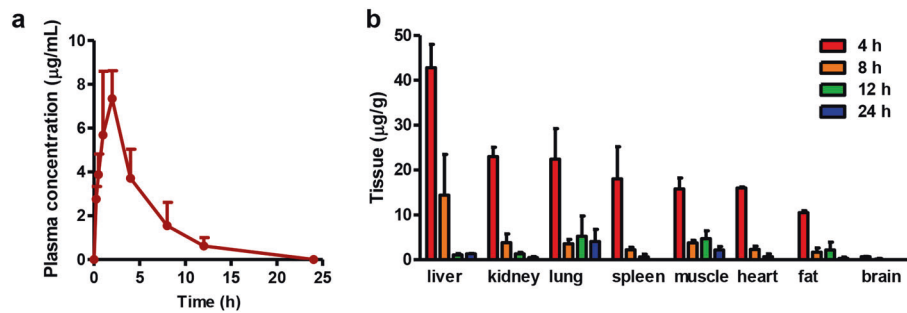


Fig. 2 Pharmacokinetics and tissue biodistribution of WZ66 in mice. **a** Pharmacokinetics of WZ66 in plasma ($n = 4$ per group). Blood was collected from each mouse at 0.25, 0.5, 1, 2, 4, 8, 12, and 24 h. **b** Tissue biodistribution of WZ66 in the liver, kidney, lung, spleen, muscle, heart, fat, and brain ($n = 8$ including four time points). Data are represented as the mean \pm SEM

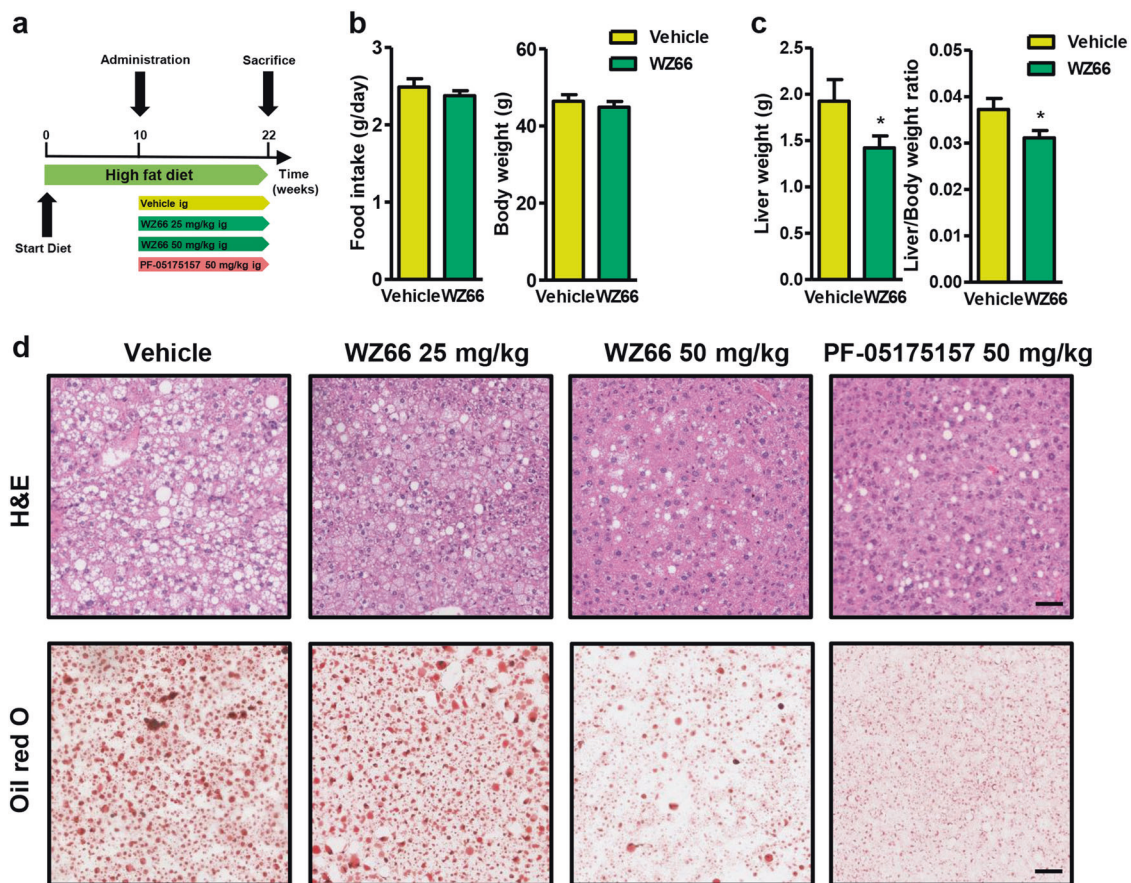


Fig. 3 WZ66 attenuated hepatic steatosis. **a** Schematic of WZ66 and PF-05175157 treatment in HFD-induced obese mice. **b** Food intake and body weights ($n = 7$ per group). **c** Liver weights and liver/body weight ratios ($n = 14$ for vehicle; $n = 13$ for WZ66). **d** Representative images of H&E and Oil red O staining of liver sections from HFD-induced obese mice with vehicle, WZ66 (25 mg/kg), WZ66 (50 mg/kg), or PF-05175157 (50 mg/kg) treatment (scale bar = 50 μ m, magnification = 20 \times). Data are represented as the mean \pm SEM. * $P < 0.05$

PC, PE, phosphatidylglycerol (PG), phosphatidylinositol (PI), sphingomyelin (SM), sphingosine (Sph), and triglycerides (TGs). Consistent with the H&E and Oil red O staining results, the lipidome analysis showed that the total lipids decreased significantly in the WZ66-treated group compared with the vehicle group (Fig. 5b). Lipids, such as DGs, PC, SM, and TGs, which have been reported to be associated with NAFLD progression [29–34], were obviously reduced in the livers of WZ66-treated mice (Fig. 5c). Moreover, 48 species of lipids out of 244 were observed with significant differences between the WZ66-treated and vehicle groups, most of which decreased; the exceptions were that PG(18:2/22:6), PG(18:1/22:6), LysoPC(20:2),

PG(18:2/16:0), PG(18:1/18:2), LysoPE(22:6), PG(18:1/20:4), SM (d42:2), and PC(36:4) (isomer 1) were increased following WZ66 treatment (Fig. 5d). Moreover, we found the gene expression levels of *Fasn*, *Elovl4*, *Elovl5*, *Cers2*, *Cers4*, *Lpin1*, *Lpin2*, and *Srebf1* were inhibited in the WZ66-treated group, suggesting the depression of DNL and sphingolipid biosynthesis in these livers (Fig. 5e). The expression levels of all genes was normalized to the vehicle group to control unwanted sources of variation. The protein expression of mature SREBP1c in the liver was similar between the WZ66-treated group and the vehicle group (Fig. 5f). Overall, our results indicated that WZ66 was able to reduce lipid accumulation in HFD-induced mouse livers.

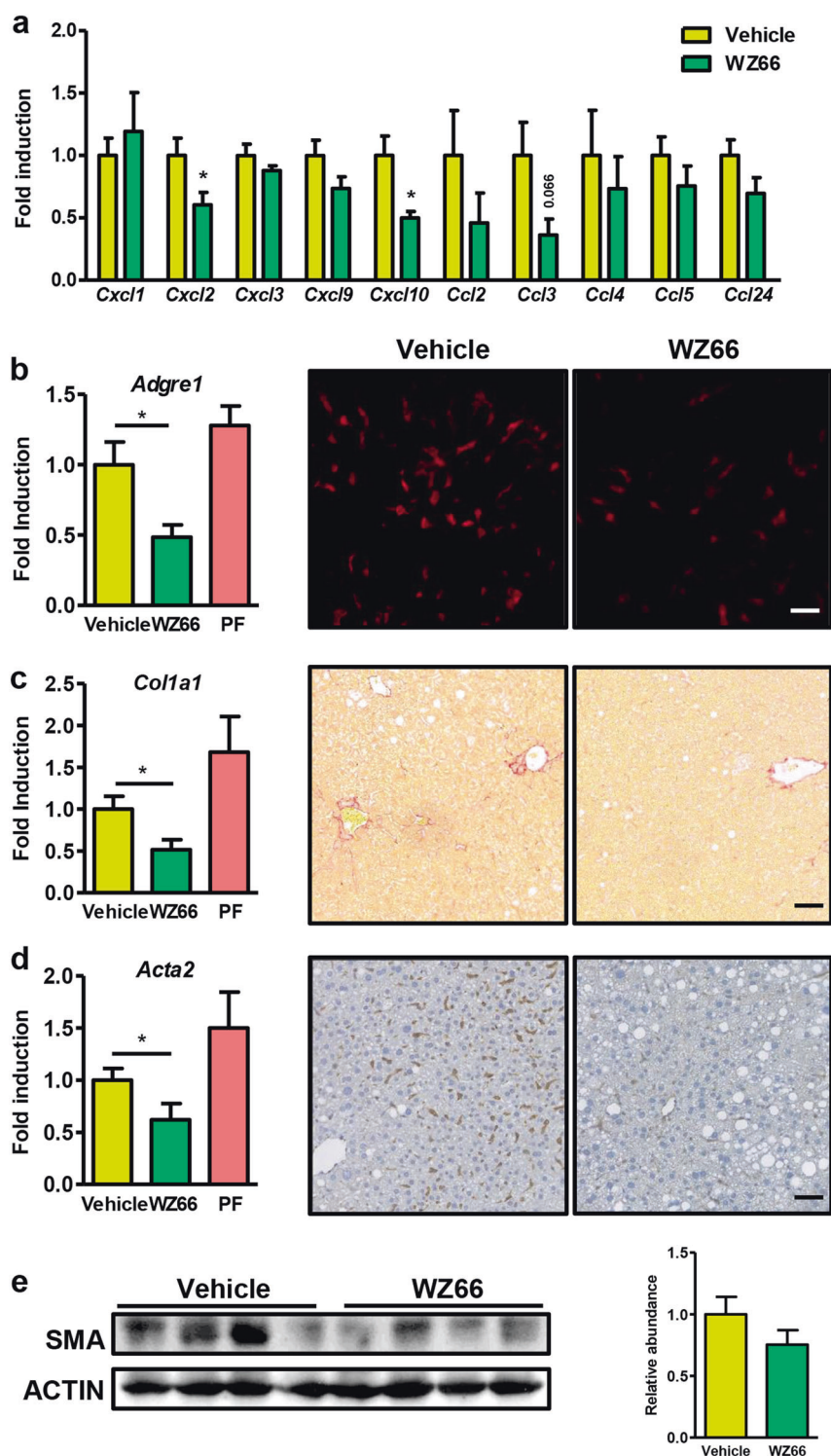


Fig. 4 WZ66 inhibited Kupffer cell activation and infiltration as well as decreased hepatic stellate cell activation. **a** Hepatic mRNA of chemokines ($n = 7$ for vehicle; $n = 6$ for WZ66). **b** (left) *Adgre1* (F4/80) mRNA level in the liver ($n = 14$ for vehicle; $n = 13$ for WZ66; $n = 10$ for PF-05175157); (right) representative images of F4/80 immunofluorescent staining of liver sections from HFD-fed obese mice with vehicle or WZ66 treatment (scale bar = 50 μm , magnification = 20 \times). **c** (left) *Col1a1* mRNA level in the liver ($n = 14$ for Vehicle; $n = 13$ for WZ66; $n = 10$ for PF-05175157); (right) representative images of sirius red staining of liver sections from obese mice with vehicle or WZ66 treatment (scale bar = 50 μm , magnification = 20 \times). **d** (left) *Acta2* mRNA level in the liver ($n = 14$ for vehicle; $n = 13$ for WZ66; $n = 10$ for PF-05175157); (right) representative images of α -SMA immunohistochemical staining of liver sections from obese mice with vehicle or WZ66 treatment (scale bar = 50 μm , magnification = 20 \times). **e** Western blot for α -SMA and quantitative analysis of the bands ($n = 4$ per group). Data are represented as the mean \pm SEM. $P < 0.05$

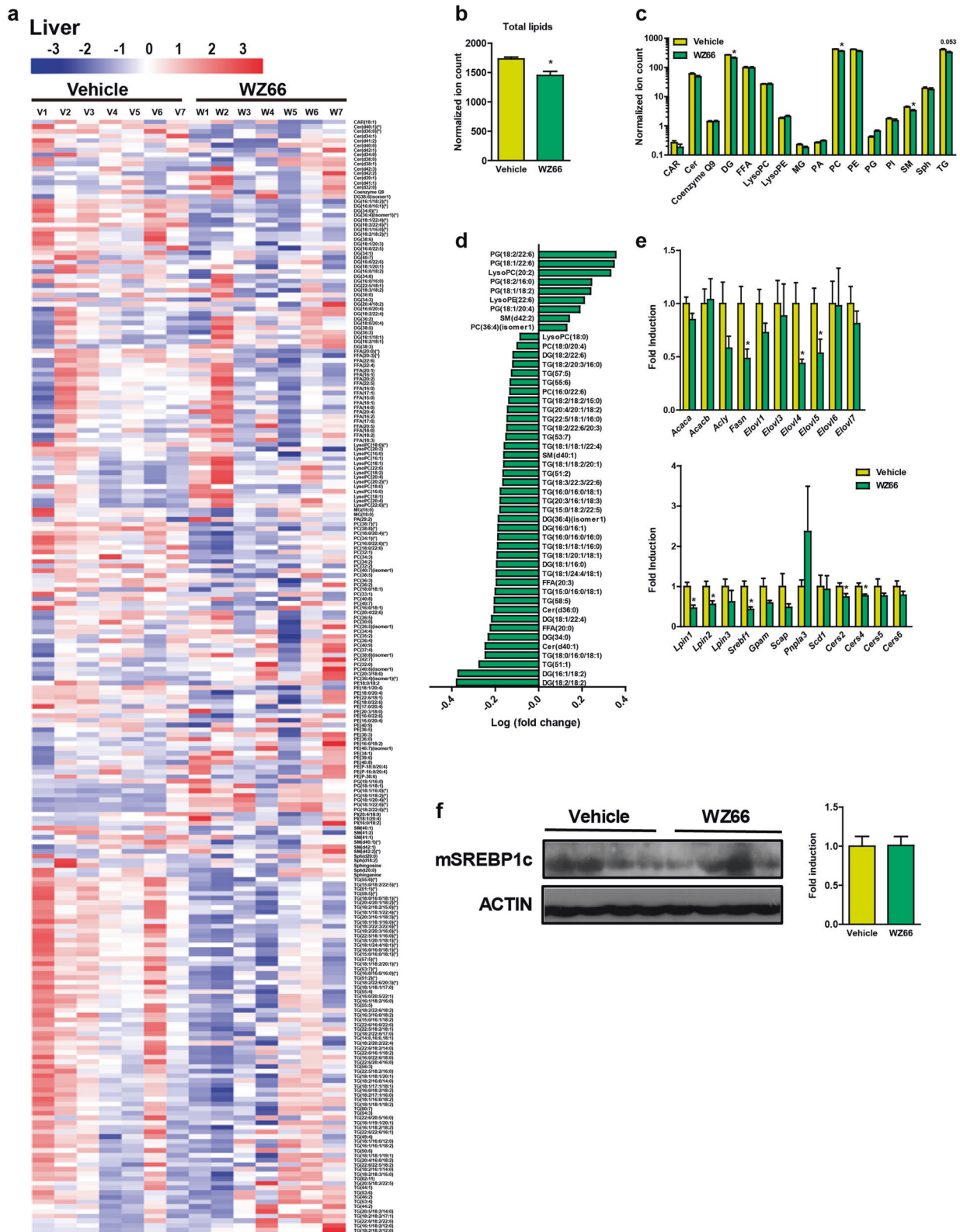


Fig. 5 Treatment with WZ66 reduced lipid accumulation in the liver. **a** Heatmap of the relative abundance of lipids in the livers from the vehicle group and WZ66-treated group ($n = 7$ per group). **b** The amount of total lipids in the livers ($n = 7$ per group). **c** The relative abundance of each class of lipids in the livers ($n = 7$ per group). **d** The lipids that changed significantly after treatment with WZ66 ($n = 7$ per group). The scale of the y-axis is presented as log10. **e** *Acaca*, *Acacb*, *Acly*, *Fasn*, *Elov1*, *Elov3*, *Elov4*, *Elov5*, *Elov6*, *Elov7*, *Lpin1*, *Lpin2*, *Lpin3*, *Sreb1*, *Gpam*, *Scap*, *Pnpla3*, *Scd1*, *Cers2*, *Cers4*, *Cers5*, and *Cers6* mRNA levels in the livers ($n = 7$ per group). **f** Western blot for mature SREBP1c and quantitative analysis of the bands ($n = 4$ per group). Data are represented as the mean \pm SEM. * $P < 0.05$

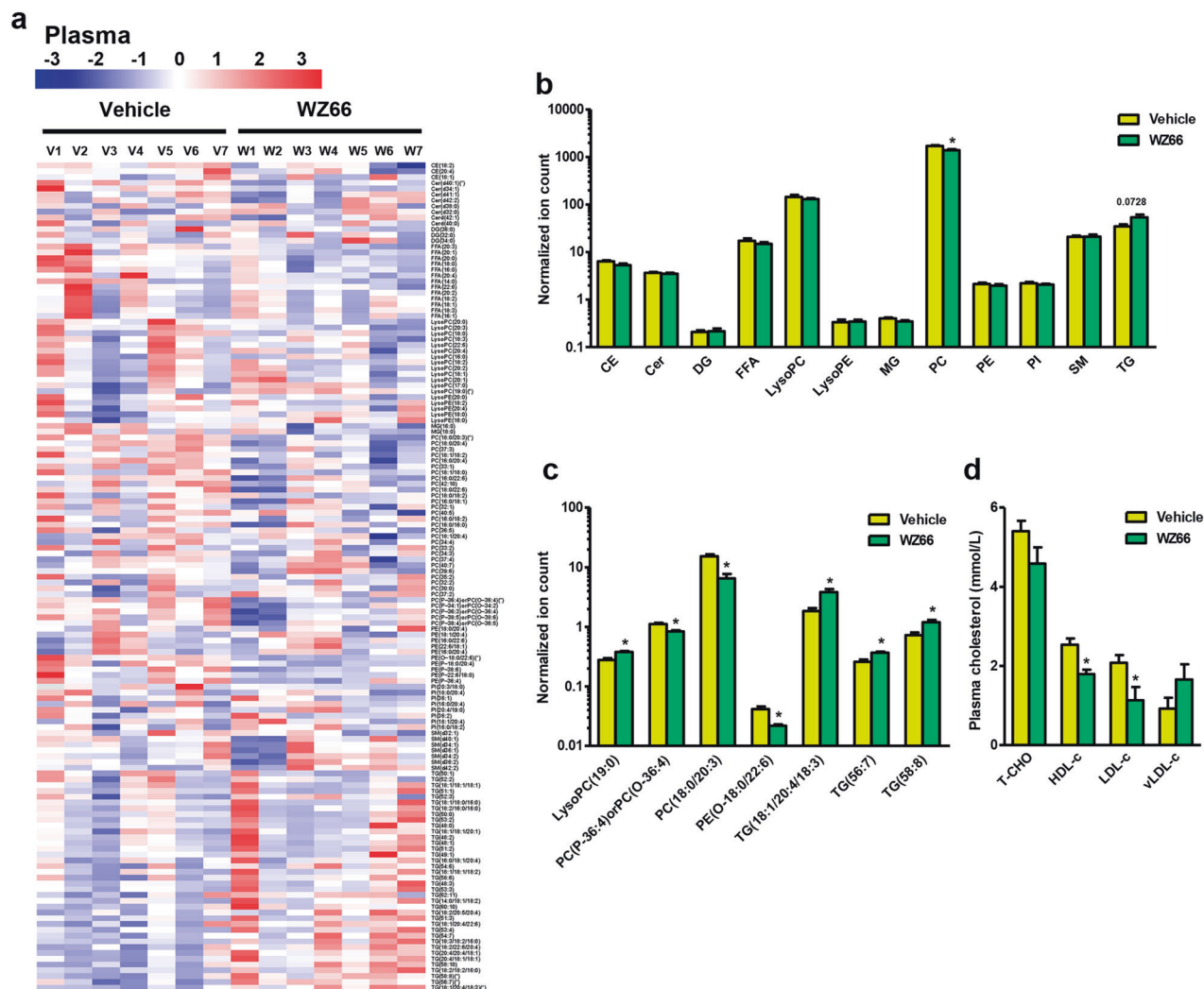


Fig. 6 WZ66 modulated the lipid profiles in plasma. **a** Heatmap of the relative abundance of the lipids in plasma ($n = 7$ per group). **b** The relative abundance of each class of lipids in plasma ($n = 7$ per group). **c** The lipids that changed significantly following treatment with WZ66 ($n = 7$ per group). The scale of the y-axis is presented as \log_{10} . **d** Total cholesterol, HDL-cholesterol, LDL-cholesterol, and vLDL-cholesterol in plasma ($n = 7$ per group). Data are represented as the mean \pm SEM. * $P < 0.05$

Lipid signatures in plasma were altered by WZ66 treatment. Untargeted lipidome analysis was also adopted to evaluate the effects of WZ66 on the plasma lipidome in HFD-induced mice (Fig. 6a). It appeared that the total PC amount in plasma obviously decreased following WZ66 treatment (Fig. 6b). The TGs in plasma showed an increasing trend ($P = 0.0728$) in WZ66-treated mice relative to control mice (Fig. 6b). In terms of alterations in specific lipids, administration of WZ66 induced higher levels of TG(18:1/20:4/18:3), TG(56:7), TG(58:8), and LysoPC(19:0), while lower levels of PC(P-36:4) or (O-36:4), PC(18:0/20:3), and PE(O-18:0/22:6) were observed in plasma (Fig. 6c). In addition, after treatment with WZ66, plasma cholesterol in LDL (LDL-c) and HDL particles (HDL-c) were lowered (Fig. 6d). Taken together, our results revealed the specific alterations in the plasma lipidome induced by WZ66 administration, among which the decreased amounts of PC, HDL-c and LDL-c and moderately increased TG levels were the notable changes.

WZ66 regulated gut microbiota composition

We performed 16S rRNA gene sequencing analysis to assess the influences of WZ66 on the gut microbiota. As shown, no significant difference in phylogenetic diversity was observed

between the WZ66-treated and vehicle mice (Fig. 7a). However, principal coordinate analysis revealed a clear separation of the microbiota diversity between WZ66-treated mice and vehicle mice (Fig. 7b). At the phylum level, the relative abundance of *Deferribacteres* decreased significantly following WZ66 treatment (Fig. 7c). At the genus level, we found that WZ66 induced a dramatic reduction in the abundance of *Allobaculum*, *Mucispirillum*, and *Prevotella* (Fig. 7d, e). Of note, the species *Mucispirillum schaedleri* was suppressed in WZ66-treated mice (Fig. 7e). Collectively, we observed alterations in the gut microbiota following WZ66 treatment.

DISCUSSION

ACCs (ACC1/2) as drug targets have attracted extensive attention in the metabolic and cancer fields in recent years [5, 14, 35, 36]. Increasing evidence has demonstrated the application of ACC inhibitors in diabetes, hepatic steatosis and hepatocellular carcinoma [5, 12, 18]. Here, we developed a novel ACC inhibitor, WZ66, which was capable of reducing hepatic steatosis, preventing macrophage and stellate cell activation as well as collagen accumulation. In addition to decreasing TGs in the liver, WZ66 also

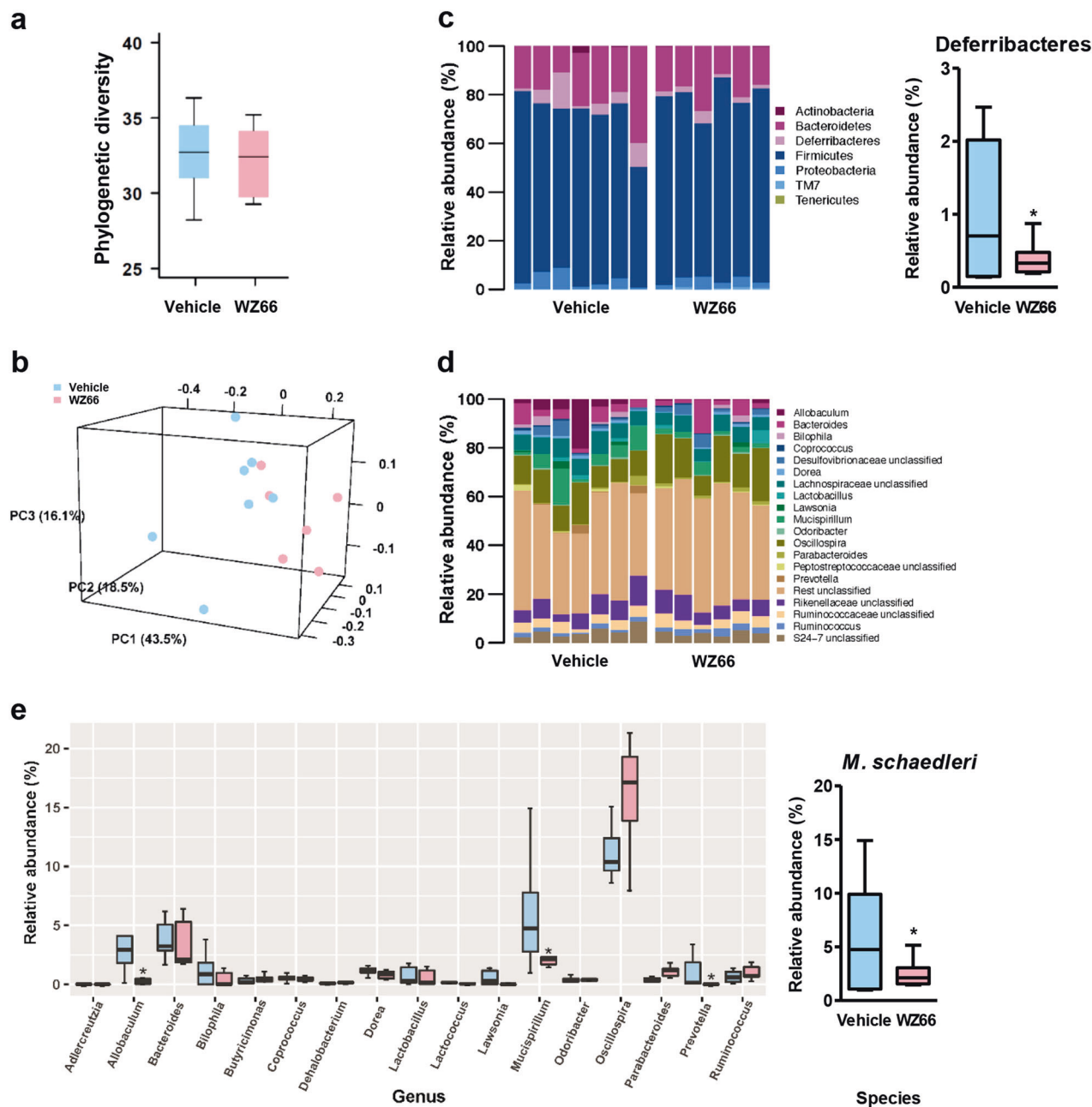


Fig. 7 WZ66 regulated the gut microbiota composition. **a** Phylogenetic diversity in diet-induced obese mice with vehicle and WZ66 treatment ($n = 7$ per group). **b** Principal component analysis (PCA) of the gut microbiota in vehicle and WZ66-treated obese mice ($n = 7$ per group). **c** (left) The relative abundance of gut microbiota at the phylum level; (right) the abundance from the phylum *Deferribacteres* decreased in WZ66-treated obese mice. **d** The relative abundance of gut microbiota at the genus level. **e** (left) The relative abundance of 17 genera with abundance >1%; the abundance of *Allobaculum*, *Mucispirillum*, and *Prevotella* were downregulated significantly between vehicle and WZ66-treated obese mice. (right) The relative abundance of *Mucispirillum schaedleri* species decreased in the WZ66-treated group. Statistical analysis was performed using the negative binomial test in the “edgeR” R package after TMM normalization, and the Benjamini & Hochberg corrected $P < 0.05$ was considered significant

lowered the levels of several toxic lipids, including DGs, PC and SM. Moreover, in addition to the ACC inhibitory activity, WZ66 also modulated the gene-expression levels of DNL, such as *Acaca* (ACC1), *Acacb* (ACC2), *Fasn*, and *Gpam* in mouse hepatocytes. WZ66 also altered the lipid profile and decreased the cholesterol levels in plasma. Finally, we further revealed that WZ66 influenced the composition of the microbiota, as shown by the decreased abundance of *Allobaculum*, *Mucispirillum*, and *Prevotella* (Fig. 8). Overall, we integrated the lipidome in the liver and plasma as well

as the gut microbiome to extensively decipher the effects of the newly identified ACC inhibitor WZ66 on the progression of NASH.

In this study, we utilized lipidome analysis to concisely detect which species of lipids were altered due to ACC inhibitor treatment. Using WZ66 as a probe, we found that DGs, PC, and SM, and TGs were the most altered lipids in the liver. The reduction in these four classes of lipids contributed to the significant decrease of the total lipids in the liver. More specifically, we elucidated 48 species of lipids out of the 244 that were

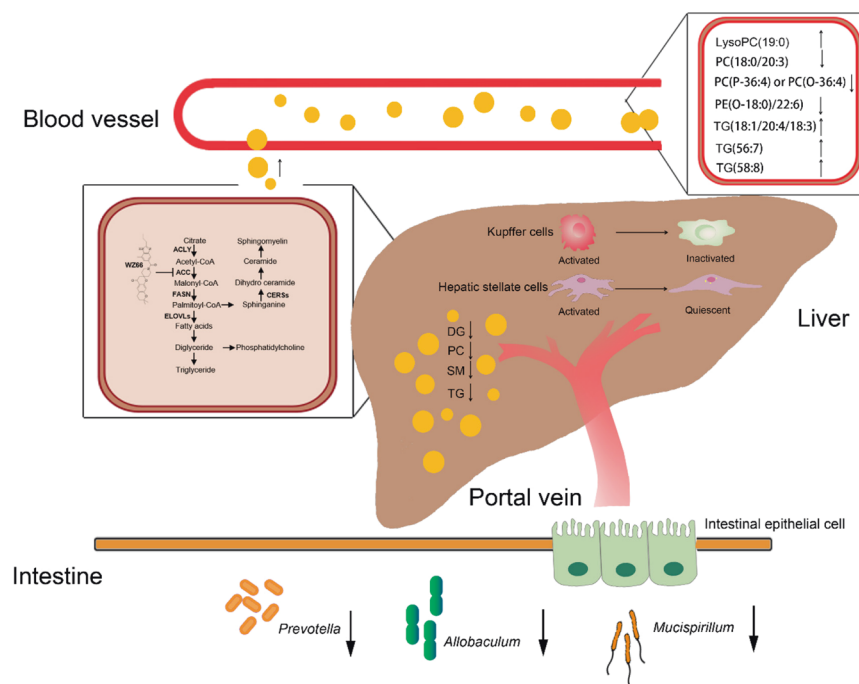


Fig. 8 A proposed working model for WZ66 in the prevention of nonalcoholic steatohepatitis (NASH). ACC inhibition by WZ66 led to a decrease in de novo lipogenesis (DNL), which was evidenced by the lowered levels of triglycerides (TGs), diglycerides (DGs), phosphatidylcholine (PC), and sphingomyelin (SM) in the liver. The reduced lipid accumulation might promote the transition of Kupffer cells and hepatic stellate cells from the activated state to the inactivate state, leading to decreased Kupffer cell activation and collagen expression. The changes in lipid profiles in the plasma caused an altered lipidome in the plasma, in which TG(18:1/20:4/18:3), TG(56:7), TG(58:8), and LysoPC(19:0) increased while PC(P-36:4) or (O-36:4), PC(18:0/20:3), and PE(O-18:0/22:6) decreased. All of the above changes due to WZ66 administration directly or indirectly induced alterations in the gut microbiota, as evidenced by the decreased abundance of the genera *Allobaculum*, *Mucispirillum*, and *Prevotella* in the intestine

modulated following WZ66 treatment. Correspondingly, the gene expression levels of the genes involved in DNL, exemplified by fatty acid biosynthesis and sphingolipid biosynthesis, were also observed to be decreased in WZ66-treated mice, providing another layer of inhibition of lipogenesis.

Recent studies have revealed that ACC inhibitors elevate plasma TGs in rodents and humans [10, 11]. The mechanism by which the TG levels increased is through reduction of malonyl-CoA levels due to ACC inhibition (resulting from chemical inhibitors or genetic deficiency) suppressing the synthesis of polyunsaturated fatty acids as exemplified by arachidonic acid (ARA) (C20:4, n-6) and docosahexaenoic acid (DHA) (C22:6, n-3), which leads to increased SREBP1c and GPAT1 expression, vLDL secretion and hypertriglyceridemia [10, 11]. Here, we found that plasma TGs, mainly TG(18:1/20:4/18:3), TG(56:7), and TG(58:8), were moderately elevated. However, FFA(20:4) and FFA(22:6), which might mainly contain ARA and DHA, were not visibly suppressed in the livers of WZ66-treated mice compared with vehicle mice, as shown in the lipidome heatmap. Furthermore, the gene and protein expression levels of SREBP1c (gene name *Srebp1*) and GPAT1 (gene name *Gpat*) were also not increased in the livers following WZ66 treatment. The discrepancies between the reported mechanism and our findings suggest that some unidentified mechanisms might warrant further investigation to explain the elevation of plasma TGs due to ACC inhibition.

Alterations in the gut microbiota were closely intertwined with the progression of NASH [15, 37]. ACCs are widely acknowledged targets of NASH [12, 13, 38]. We therefore examined the regulation of gut microbiota resulting from ACC inhibition. The relative abundance of the genera *Allobaculum*, *Mucispirillum*, and *Prevotella* and the species *Mucispirillum schaedleri* decreased in WZ66-treated mice relative to vehicle mice. As reported, the genus *Mucispirillum* and species *Mucispirillum schaedleri* have widely

been associated with intestinal inflammation [39]; thus, WZ66 might provide beneficial effects to the intestine. It should be noted that we could not discriminate that the alterations to the gut microbiota resulted from ACC inhibition in the liver or in the intestine, where ACCs are also expressed [40].

Knockout mice with target deficiency were employed to validate the specificity of the effects induced by WZ66 in vivo. However, the hepatocyte-specific ACC1/ACC2 deficiency protected mice from diet-induced hepatic steatosis per se [11], making it impossible to demonstrate that the decreased effects of WZ66 on NASH observed in this study were abolished in ACC1/2-deficient mice. In conclusion, we identified a novel ACC inhibitor, WZ66, and demonstrated that it efficiently attenuated hepatic steatosis and inhibited macrophage and hepatic stellate cell activation as well as collagen accumulation, indicating that WZ66 might be used as a lead compound or drug candidate for the treatment of NASH and its end stage diseases, including liver cirrhosis and hepatocellular carcinoma.

ACKNOWLEDGEMENTS

This study was supported by the National Natural Science Foundation of China (81700748 to LRW), by funding the “Double First-Class” University Project (CPU2018GF10 to LRW and CPU2018GY31 to LRW) and “National Key R&D Program of China” (2018YFC1704900 and 2018YFC1704905 to LRW).

AUTHOR CONTRIBUTIONS

YSG and MYQ were responsible for the design of the experiments, acquisition of the data, analysis and interpretation of the data, and the writing of the paper; XBD, JL, CYP, and SQZ assisted in animal feeding and data collection; SLW and LWQ were responsible for collection and analysis of the lipidome; HYH was responsible for the data analysis of the 16S rRNA and lipidome; QQW, JPZ., and HBZ provided WZ66; HBZ

and LRW were responsible for the study concept and design, revising the paper, and study supervision.

ADDITIONAL INFORMATION

The online version of this article (<https://doi.org/10.1038/s41401-019-0310-0>) contains supplementary material, which is available to authorized users.

Competing interests: The authors declare no competing interests.

Publisher's note Springer Nature remains neutral with regard to jurisdictional claims in published maps and institutional affiliations.

REFERENCES

- Musso G, Cassader M, Gambino R. Non-alcoholic steatohepatitis: emerging molecular targets and therapeutic strategies. *Nat Rev Drug Discov.* 2016;15:249–74.
- Cassidy S, Syed BA. Nonalcoholic steatohepatitis (NASH) drugs market. *Nat Rev Drug Discov.* 2016;15:745–46.
- Pellicoro A, Ramachandran P, Iredale JP, Fallowfield JA. Liver fibrosis and repair: immune regulation of wound healing in a solid organ. *Nat Rev Immunol.* 2014;14:181–94.
- Diehl AM, Day C. Cause, pathogenesis, and treatment of nonalcoholic steatohepatitis. *N Engl J Med.* 2017;377:2063–72.
- Harriman G, Greenwood J, Bhat S, Huang X, Wang R, Paul D, et al. Acetyl-CoA carboxylase inhibition by ND-630 reduces hepatic steatosis, improves insulin sensitivity, and modulates dyslipidemia in rats. *Proc Natl Acad Sci U S A.* 2016;113:E1796–805.
- Wei J, Tong L. Crystal structure of the 500-kDa yeast acetyl-CoA carboxylase holoenzyme dimer. *Nature.* 2015;526:723–7.
- Wakil SJ, Abu-Elheiga LA. Fatty acid metabolism: target for metabolic syndrome. *J Lipid Res.* 2009;50:Suppl: S138–43.
- Thampy KG, Wakil SJ. Regulation of acetyl-coenzyme A carboxylase. I. Purification and properties of two forms of acetyl-coenzyme A carboxylase from rat liver. *J Biol Chem.* 1988;263:6447–53.
- Abu-Elheiga L, Brinkley WR, Zhong L, Chirala SS, Woldegiorgis G, Wakil SJ. The subcellular localization of acetyl-CoA carboxylase 2. *Proc Natl Acad Sci U S A.* 2000;97:1444–9.
- Goedeke L, Bates J, Vatner DF, Perry RJ, Wang T, Ramirez R, et al. Acetyl-CoA carboxylase inhibition reverses NAFLD and hepatic insulin resistance but promotes hypertriglyceridemia in rodents. *Hepatology.* 2018;68:2197–211.
- Kim CW, Addy C, Kusunoki J, Anderson NN, Deja S, Fu X, et al. Acetyl CoA carboxylase inhibition reduces hepatic steatosis but elevates plasma triglycerides in mice and humans: a bedside to bench investigation. *Cell Metab.* 2017;26:576.
- Lally JSV, Ghoshal S, DePeralta DK, Moaven O, Wei L, Masia R, et al. Inhibition of acetyl-CoA carboxylase by phosphorylation or the inhibitor ND-654 suppresses lipogenesis and hepatocellular carcinoma. *Cell Metab.* 2019;29:174–82 e5.
- Lawitz EJ, Coste A, Poordad F, Alkhoury N, Loo N, McColgan BJ, et al. Acetyl-CoA carboxylase inhibitor GS-0976 for 12 weeks reduces hepatic de novo lipogenesis and steatosis in patients with nonalcoholic steatohepatitis. *Clin Gastroenterol Hepatol.* 2018;16:1983–91 e3.
- Svensson RU, Parker SJ, Eichner LJ, Kolar MJ, Wallace M, Brun SN, et al. Inhibition of acetyl-CoA carboxylase suppresses fatty acid synthesis and tumor growth of non-small-cell lung cancer in preclinical models. *Nat Med.* 2016;22:1108–19.
- Boursier J, Mueller O, Barret M, Machado M, Fizanne L, Araujo-Perez F, et al. The severity of nonalcoholic fatty liver disease is associated with gut dysbiosis and shift in the metabolic function of the gut microbiota. *Hepatology.* 2016;63:764–75.
- Zhu L, Baker SS, Gill C, Liu W, Alkhoury R, Baker RD, et al. Characterization of gut microbiomes in nonalcoholic steatohepatitis (NASH) patients: a connection between endogenous alcohol and NASH. *Hepatology.* 2013;57:601–9.
- Tsuchiya H, Ebata Y, Sakabe T, Hama S, Kogure K, Shiota G. High-fat, high-fructose diet induces hepatic iron overload via a hepcidin-independent mechanism prior to the onset of liver steatosis and insulin resistance in mice. *Metabolism.* 2013;62:62–9.
- Griffith DA, Kung DW, Esler WP, Amor PA, Bagley SW, Beysen C, et al. Decreasing the rate of metabolic ketone reduction in the discovery of a clinical acetyl-CoA carboxylase inhibitor for the treatment of diabetes. *J Med Chem.* 2014;57:10512–26.
- Kung DW, Griffith DA, Esler WP, Vajdos FF, Mathiowetz AM, Doran SD, et al. Discovery of spirocyclic-diamine inhibitors of mammalian acetyl CoA-carboxylase. *Bioorg Med Chem Lett.* 2015;25:5352–6.
- Yang Y, Zhao L, Xu B, Yang L, Zhang J, Zhang H, et al. Design, synthesis and biological evaluation of dihydroquinoxalione derivatives as BRD4 inhibitors. *Bioorg Chem.* 2016;68:236–44.
- Mazagova M, Wang L, Anfora AT, Wissmueller M, Lesley SA, Miyamoto Y, et al. Commensal microbiota is hepatoprotective and prevents liver fibrosis in mice. *FASEB J.* 2015;29:1043–55.
- Wang L, Fouts DE, Starkel P, Hartmann P, Chen P, Llorente C, et al. Intestinal REG3 lectins protect against alcoholic steatohepatitis by reducing mucosa-associated microbiota and preventing bacterial translocation. *Cell Host Microbe.* 2016;19:227–39.
- Leuthold P, Schaeffeler E, Winter S, Buttner F, Hofmann U, Mordt TE, et al. Comprehensive metabolomic and lipidomic profiling of human kidney tissue: a platform comparison. *J Proteome Res.* 2017;16:933–44.
- Want EJ, Masson P, Michopoulos F, Wilson ID, Theodoridis G, Plumb RS, et al. Global metabolic profiling of animal and human tissues via UPLC-MS. *Nat Protoc.* 2013;8:17–32.
- Wang L, Hu C, Liu S, Chang M, Gao P, Wang L, et al. Plasma lipidomics investigation of hemodialysis effects by using liquid chromatography-mass spectrometry. *J Proteome Res.* 2016;15:1986–94.
- Fahy E, Sud M, Cotter D, Subramaniam S. LIPID MAPS online tools for lipid research. *Nucleic Acids Res.* 2007;35(Web Server issue):W606–12.
- Llorente C, Jepsen P, Inamine T, Wang L, Bluemel S, Wang HJ, et al. Gastric acid suppression promotes alcoholic liver disease by inducing overgrowth of intestinal *Enterococcus*. *Nat Commun.* 2017;8:837.
- Bokulich NA, Dillon MR, Zhang Y, Rideout JR, Bolyen E, Li H, et al. q2-longitudinal: longitudinal and paired-sample analyses of microbiome data. *mSystems.* 2018;3:e00219–18. pii
- Puri P, Baillie RA, Wiest MM, Mirshahi F, Choudhury J, Cheung O, et al. A lipidomic analysis of nonalcoholic fatty liver disease. *Hepatology.* 2007;46:1081–90.
- Van der Veen JN, Kennelly JP, Wan S, Vance JE, Vance DE, Jacobs RL. The critical role of phosphatidylcholine and phosphatidylethanolamine metabolism in health and disease. *Biochim Biophys Acta Biomembr.* 2017;1859(9 Pt B):1558–72.
- Apostolopoulou M, Gordillo R, Koliaki C, Gancheva S, Jelenik T, De Filippo E, et al. Specific hepatic sphingolipids relate to insulin resistance, oxidative stress, and inflammation in nonalcoholic steatohepatitis. *Diabetes Care.* 2018;41:1235–43.
- Ikura Y, Ohsawa M, Suekane T, Fukushima H, Itabe H, Jomura H, et al. Localization of oxidized phosphatidylcholine in nonalcoholic fatty liver disease: impact on disease progression. *Hepatology.* 2006;43:506–14.
- Li Z, Agellon LB, Allen TM, Umeda M, Jewell L, Mason A, et al. The ratio of phosphatidylcholine to phosphatidylethanolamine influences membrane integrity and steatohepatitis. *Cell Metab.* 2006;3:321–31.
- Marra F, Svegliati-Baroni G. Lipotoxicity and the gut-liver axis in NASH pathogenesis. *J Hepatol.* 2018;68:280–95.
- Tong L, Harwood HJ Jr. Acetyl-coenzyme A carboxylases: versatile targets for drug discovery. *J Cell Biochem.* 2006;99:1476–88.
- Bourbeau MP, Bartberger MD. Recent advances in the development of acetyl-CoA carboxylase (ACC) inhibitors for the treatment of metabolic disease. *J Med Chem.* 2015;58:525–36.
- Leung C, Rivera L, Furness JB, Angus PW. The role of the gut microbiota in NAFLD. *Nat Rev Gastroenterol Hepatol.* 2016;13:412–25.
- Loomba R, Kayali Z, Nouredin M, Ruane P, Lawitz EJ, Bennett M, et al. GS-0976 reduces hepatic steatosis and fibrosis markers in patients with nonalcoholic fatty liver disease. *Gastroenterology.* 2018;155:1463–73 e6.
- Berry D, Schwab C, Milinovich G, Reichert J, Ben Mahfoudh K, Decker T, et al. Phylogeny-level 16S rRNA analysis reveals new bacterial indicators of health state in acute murine colitis. *ISME J.* 2012;6:2091–106.
- Field FJ, Born E, Mathur SN. Fatty acid flux suppresses fatty acid synthesis in hamster intestine independently of SREBP-1 expression. *J Lipid Res.* 2003;44:1199–208.